ORIGINAL ARTICLE

Effects of silane concentration on hydrophobic conversion of rice husk-derived silica aerogels prepared by supercritical drying

Zulhelmi Alif Abd Halim[1] · Nuha Awang[2] · Norhayati Ahmad[1] · Muhamad Azizi Mat Yajid[1]

Abstract

Supercritical fluid drying (SCFD) and ambient pressure drying (APD) are two common drying methods in the synthesis of silica aerogels (SA). The SCFD efficiently produces high-quality SA with good reproducibility, however, the produced SA is hydrophilic and has poor moisture tolerance. Meanwhile, the APD is less energy-intensive process but requires an extra amount of organic solvents and hydrophobic silanes to effectively control drying shrinkage. In this study, a new route for synthesizing hydrophobic SA is proposed, using rice husk-derived sodium silicate as a cheap precursor and without the need for high amounts of chemical reagent. First, hydrophilic SA particles (100 µm to 1.0 mm) with a large specific surface area (700 m^2/g) were produced using a sol–gel method, ethanol solvent exchange, and SCFD drying. The dried hydrophilic SA were then surface hydrophobized by simple immersion in a silane reagent containing 2%, 5%, and 10% trimethylchlorosilane (TMCS) in n-hexane. These concentration of TMCS was at least ten times lower than that required by the standard APD approach, reducing chemical waste. The TMCS-modified SA shrank by 9.0–17% compared to the original SA, which slightly increasing their final density and thermal conductivity. Hydrophobization was most effective at 5% TMCS, as indicated by the largest surface area (664 m^2/g), lowest thermal conductivity (0.038 W/mK), and highest water contact angle ($\theta = 140°$). The hydrophobic SA is more thermally stable than the hydrophilic SA, which can resist temperatures as high as 350 °C.

Keywords Rice husk · Silica · Aerogels · Hydrophobic · Supercritical drying

1 Introduction

Burning rice remnants (straws and husks) in the paddy field for the following crop cycle is a typical postharvest technique in many rice-growing regions. Consequently, such open-air burning causes air pollution and contributes to global warming by producing greenhouse gases (GHGs) [1]. Due to its high calorific value and silica content, rice husk has recently been considered as desirable by companies and academia for use in renewable energy and green chemistry strategies [2]. The composition of well-burnt rice husk ash (RHA) contains more than 90% silica (SiO$_2$), the greatest percentage of any biomass [3]. Silica is easily recovered from RHA as sodium silicate by dissolving it in aqueous sodium hydroxide solution. The production of sodium silicate from RHA as a precursor of silica aerogels (SA) is a cost-effective alternative to more expensive alkoxide precursors such as Tetraethoxysilane (TEOS) [3]. SA are one of the most intriguing materials of the twenty-first century because to their excellent physical features such as low density (0.003–0.35 g/cm3), large porosity (90–96%), high surface area (400–1000 m2/g), and low thermal conductivity (0.01–0.1 W/mK), depending on their porous structure [4].

SA could be applied in a variety of applications, including adsorbents, catalysts, fillers, carriers, and dielectrics. Recently, SA are frequently proposed as fillers for high-performance thermal insulation composites where lightweightness is critical [5–7]. SA made from TEOS is one of the most common types, while SA made from RHA, despite being much cheaper, is less well-known because it is rarely commercialized. Scholarly research on the applicability of RHA-derived SA could assist reduce the cost of thermal

✉ Zulhelmi Alif Abd Halim
  zulhelmialif@gmail.com

1 Department of Materials, Manufacturing and Industrial Engineering, Faculty of Mechanical Engineering, Universiti Teknologi Malaysia, 81310 Johor Bahru, Malaysia

2 Facilities and Maintenance Engineering Section, Malaysian Institute of Industrial Technology, Universiti Kuala Lumpur, Persiaran Sinaran Ilmu, Bandar Seri Alam, 81750 Johor, Malaysia

insulation retrofits in the near future, providing it a competitive edge over other insulation materials like fiberglass and mineral wool [7]. Synthesis of SA via the sol–gel technique using sodium silicate as precursor is a well-known low-cost method. The first step in the sol–gel process is to add the right amount of acid to a sodium silicate solution to make colloidal silica. With the right solvent exchange and hydration process, porous silica gel will cross-link to form a wet silica gels or hydrogel. The drying of the hydrogel, which involves the removal of pore fluids, is a critical step in the production of an aerogel. The drying process must be controlled to optimize the SA's surface area and pore size, which govern its physical properties such as thermal conductivity [7].

Two types of methods for drying hydrogel into SA are supercritical fluid drying (SCFD) and ambient pressure drying (APD). Through distinct mechanisms, the purpose of both techniques is to eliminate capillary tension and shrinkage during evaporative drying of the hydrogel. The SCFD uses high temperatures and pressure to transform the solvent in hydrogel into a supercritical state that has no surface tension [8, 9]. Although the SCFD is sometimes criticized due to energy-intensive process, it is undeniably efficient in controlling the qualities of SA, offering high yield and low waste [8, 9]. The APD method, on the other hand, uses chemical modification to control shrinkage caused by drying-induced capillary forces. Although it is a less energy-intensive, the APD approach needs extensive chemical solvents and silanes for surface hydrophobization of the hydrogel. Trimethylchlorosilane (TMCS) is widely used silane as a surface hydrophobization agent due to its high silylation tendencies. Previous research has demonstrated the use of TMCS as a silane agent with ethanol/n-hexane [10–15] and methanol/n-hexane [16, 17] as its co-solvents. After tedious solvent exchange process, the APD approach can create hydrophobic SA of excellent quality, but the significant consumption of TMCS and co-solvents can result in high costs and negative environmental implications. In comparison, the SCFD process requires only a single solvent, such as ethanol, throughout the process, but the main disadvantage is that the SA synthesized by this method are typically hydrophilic or partially hydrophobic. Despite the fact that hydrophilic and hydrophobic SA have identical characteristics, the majority of end users avoid hydrophilic SA due to its moisture sensitivity.

Recently, more research has focused on improving the APD method for synthesizing hydrophobic SA as a result of the low demand for hydrophilic SA. To keep the SCFD technology relevant in this field, this paper proposes a straightforward process for the conversion of hydrophilic SA to hydrophobic via a simple silylation process. In this experiment, the dry SA particles obtained from the SCFD have been silylated in a TMCS/n-hexane solution dried at ambient temperature. This post-SCFD silane treatment has never been tried, hence the aim of this study is to look into the impact of different TMCS concentrations on the physicochemical changes in TMCS-silylated SA. This silylation technique is cost-effective for fine-tuning SA hydrophobicity since significantly less silane is consumed than in the conventional APD route but at the expense of a slight loss in density and thermal conductivity. The generality of this post-synthesis silane treatment may broaden the use of the SCFD approach for manufacturing high-quality, hydrophobic SA with a competitive advantage over the conventional APD method.

2 Experimental

2.1 Materials

Rice husks were obtained from a local rice mill. To prepare the sodium silicate solution, 99% sodium hydroxide (NaOH, 40 g/mol, Qrec Malaysia) was used. Hydrochloric acid 37% (HCl, Qrec Malaysia) was used as an acid catalyst for gelation, anhydrous ethanol 95% (EtOH) was used as an exchanging solvent, n-hexane 95% (Qrec, Malaysia) was used as a silylating solvent, and TMCS 98% (Tokyo Chemical Industries, Japan) was used as silane reagent. Distilled water was used to prepare the silicate sol and to wash the wet gels. The schematic of the SCFD reactor used in this investigation is shown in Fig. 1. SCFD was performed in a 2 L autoclave reactor (Parr Instrument Company, USA) utilizing pure nitrogen (N_2) as purging gas.

2.2 Production of hydrophilic SA via SCFD route

The flow diagram for the synthesis of SA and subsequent hydrophobic conversion is shown in Fig. 2. Rice husks with an average length of 10–12 mm were burned at 600 °C in a screw-type incinerator (Spaggiari Transmissiani, Italy, Model: 0,008,754, Type: SW7105). This process degrades all carbohydrates in rice husk that resulted in fine white rice husk ash (RHA) with very few carbon contents [18]. The sodium silicate solution (Na_2O: SiO_2 molar ratio of 1: 3.33) was made by dissolving 38 g of white RHA in 200 mL of 0.75 M NaOH solution and heating to reflux for 2 h at 100 °C. Filtration was used to remove solid residue from the resultant solution. The pH of the diluted silicate solution was then reduced to 5.5 by gradually adding a sufficient amount of concentrated hydrochloric acid (HCl) while pH correction can be accomplished with aqueous ammonia. The solution was gently stirred until it gels, then the generated hydrogels were immersed in warm water (50 °C) for 3 h. The water contained in the hydrogels was exchanged with ethanol (EtOH) to form alcogels using Soxhlet extraction method for 16 h. Following that, the alcogels with excess ethanol were supercritical dried in a high-pressure autoclave

Fig. 1 Schematic representation of 2 L SCFD autoclave reactor
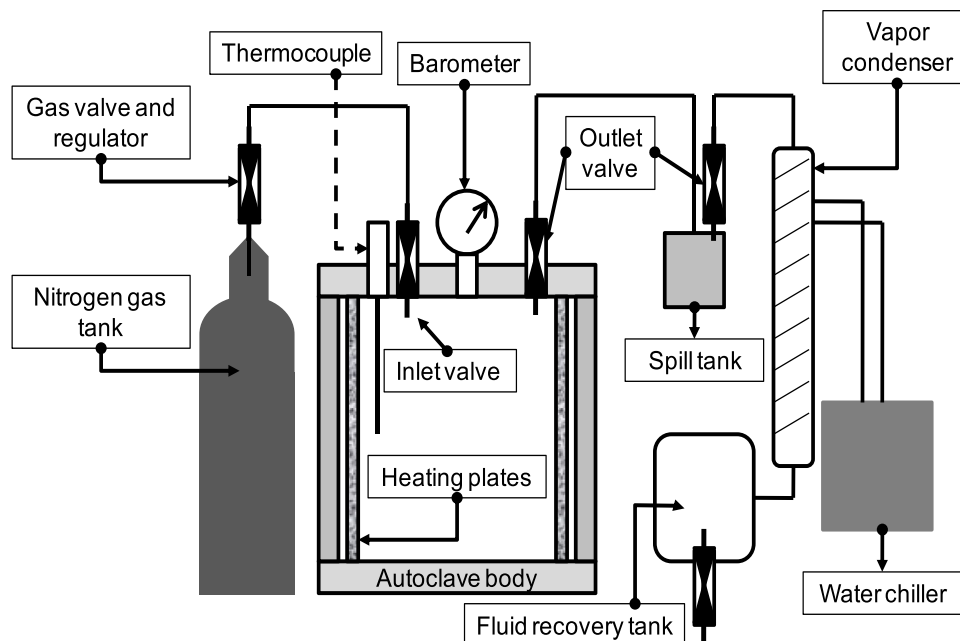
at a volume ratio of 3:5 (alcogel:ethanol). The autoclave temperature was gradually increased to 275 °C and maintained until the autoclave pressure exceeded 60 bar. The supercritical condition was maintained for at least 1 h while N_2 gas was introduced. Finally, the autoclave's ethanol vapor was gently bled until the pressure dropped to air and the SA were collected. The diameter of SA particles is generally less than 3.0 mm, mostly in the range from 100 μm to 1.0 mm.

2.3 Hydrophobic conversion of hydrophilic SA

Despite being free of water, the SA particles synthesized from the SCFD method still have water-attracting hydroxyls (silanol) attached to their surfaces, making them hydrophilic. To become hydrophobic, the Si–OH groups on the SA surface must be capped or replaced by hydrophobic entities from the TMCS, as depicted in Fig. 3. During surface silylation, Si–CH$_3$ groups will be covalently bonded to the SA surface at silanol sites, releasing hydrochloric acid (HCL) [16]. These hydrocarbon substituents form a non-polar interphase, resulting in a surface hydrophobic coating. The success of this surface modification process is due to the fact that the dry SA particles as shown in Fig. 4 have pores that were already free of water and other polar solvents. In contrast, ambient pressure drying of wet silica gels (Fig. 4) requires an extra amount of TMCS to successfully prevent shrinkage due to the presence of water within the gel's pores. Consequently, a smaller TMCS concentration is sufficient to render the SA hydrophobic since TMCS entities have greater accessibility to the surface silanol groups. In this study, three different concentrations of TMCS in n-hexane solution were prepared for surface hydrophobization: 2, 5, and 10% by

volume. For each TMCS concentration, 200 mL of dry SA particles in mesh bags were submerged in 100 mL of n-hexane solution for 15 min without agitation. Following that, the bags were drained and washed for 5 min in 100 mL of new n-hexane. The TMCS-silylated SA samples were then dried for 10 min on a hot plate in a fume hood at 120 °C, followed by 24 h in an air oven at 90 °C to ensure full evaporation of the solvent. The TMCS-silylated SA retain most of their porous structure (i.e., spring back effect) after drying.

2.4 Characterization

The bulk density of SA was determined by dividing the mass, as determined by a microbalance (Mettler Toledo, USA, precision 0.001 g), by the volume ratio. The specific surface area of SA was determined using a Monosorb surface-area analyzer utilizing the single-point BET method (Quantachrome Corp. USA). The TMCS modification of the SA causes structural shrinkage proportional to the decrease in specific surface area. The rate of shrinkage is calculated using the following formula:

$$\text{Shrinkage rate (\%)} = \left(1 - \frac{SSA_n}{SSA_o} \right) \times 100$$

where SSA is the specific surface area in m^2/g, **n** is the SA sample treated with **n**% TMCS, and **o** is the original SA sample (0% TMCS). Scanning Electron Microscopy was used to examine the microstructure and morphology (SEM, Hitachi SU3500, Japan). Attenuated transmission reflectance – Fourier transforms infrared spectroscopy was used to characterize the chemical bonds present in the SA (ATR-FTIR, Perkin Elmer,
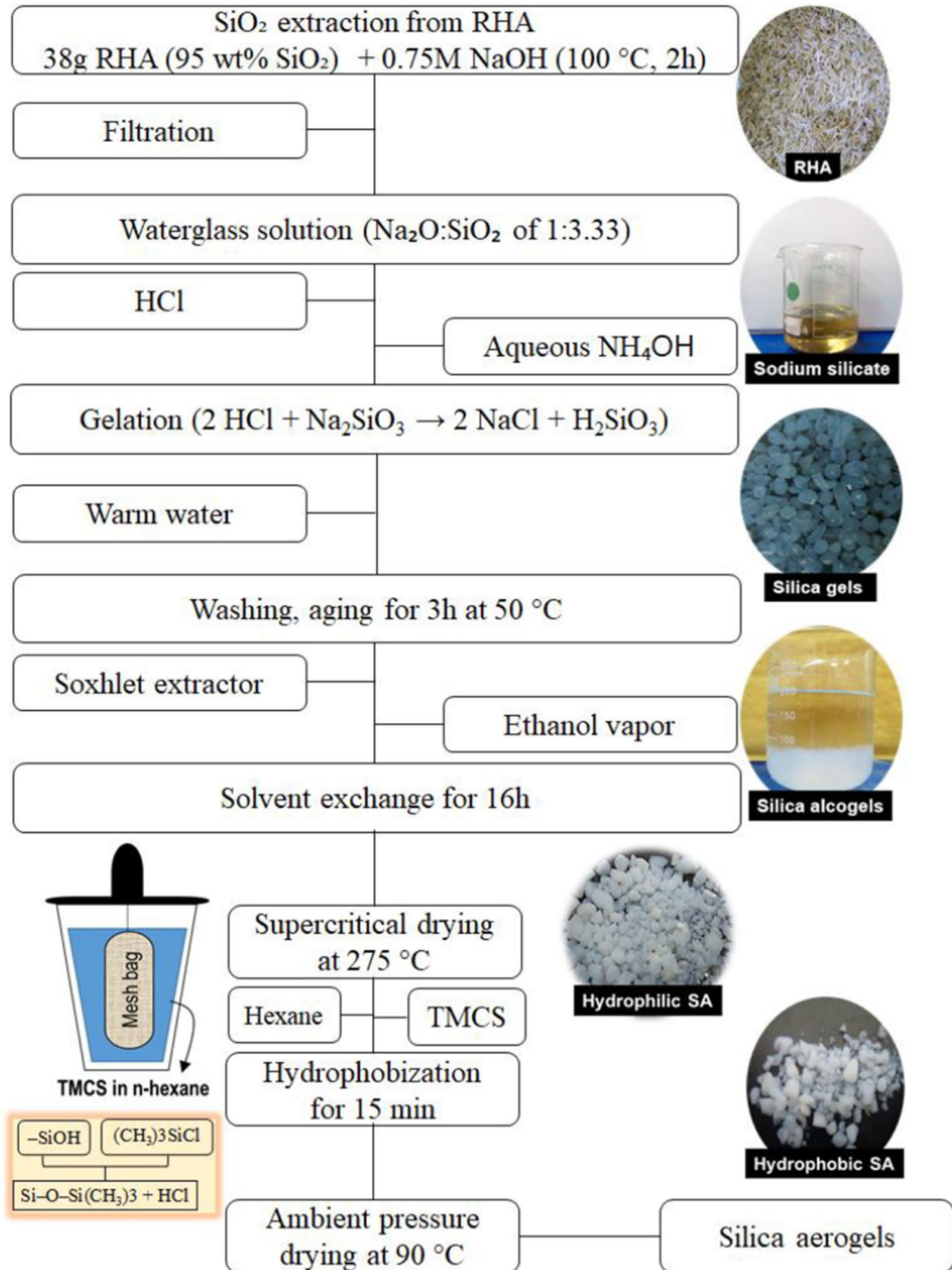
Fig. 2 Flow chart for preparation of SA from RHA

Fig. 3 Reaction between TMCS and surface silanol groups of SA
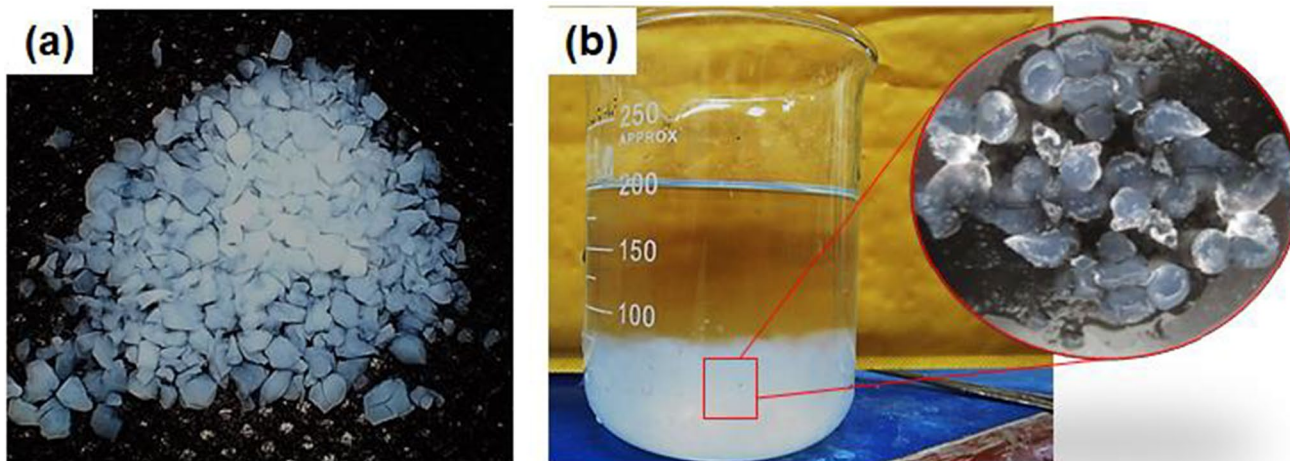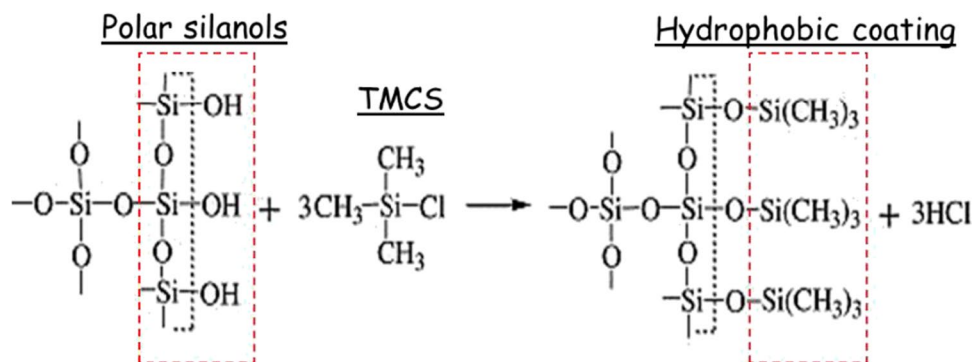

Fig. 4 Photographs of **a** dry SA particles after SCFD process (diameter range 100 μm–1.0 mm) **b** wet sol–gel derived silica gels (bead form)

USA). The degree of hydrophobicity was determined using the water contact angle technique. A known-volume water droplet is deposited on a flat surface coated with SA and the contact angle is determined using a contact angle goniometer (OCA Instruments, Germany). The thermal conductivity of SA samples was evaluated using the hot disk method at 25 °C (Hot Disk-TPS 2500S, Sweeden). For each measurement, 4 mL of SA particles were stored in a cylindrical sample holder (testing cell) without compaction. The sensor was a 10 μm thick nickel foil with a double spiral pattern embedded in Kapton polyimide film (design: 5465; radius: 3.189) that was placed into the testing cell. The thermal degradation and stability of the SA was determined by thermogravimetric analysis (TGA; Mettler Toledo, USA), which involved heating the SA sample to 600 °C in the presence of a 25 mL/min airflow.

3 Results and discussions

3.1 Effects of TMCS on physical properties

The TMCS surface modification procedure used in this study involved wetting the dry SA (from the SCFD) in

Table 1 Density, specific surface area, and calculated shrinkage of SA before and after silylation

TMCS %	Density (g/cm^3)[a]	Specific surface area (m^2/g)[b]	Shrinkage %
0	0.075 ± 0.004	715 ± 14	Original
2	0.077 ± 0.002	637 ± 13	14 ± 1.5
5	0.076 ± 0.003	664 ± 13	9.0 ± 1.0
10	0.080 ± 0.003	619 ± 12	17.0 ± 1.6

[a]The number of measurements for each SA sample is 5
[b]The number of measurements for each SA sample is 3

TMCS solution, followed by evaporative drying under ambient conditions. This wetting and drying process, however, causes small capillary pressure, which slightly reduces the dimension of interior pores, causing the surface area and bulk volume to shrink microscopically. The densities and BET surface areas of the SA samples, as given in Table 1, indicate that the TMCS silylated SA samples experienced minor shrinkage after ambient drying. The 10% TMCS sample experienced the most shrinkage, whereas the 5% TMCS sample had the least.

Microscopically, the SEM images in Fig. 5 compare the original microstructures of the SA and after modified with 10% TMCS, that results in highest shrinkage. The high magnification micrographs generally reveal the three-dimensional network of silica particles, showing the typical mesoporous structure of aerogels, with the dark spots representing the internal pores. Although not obvious, it can be seen that the surface of the original SA (Fig. 5a) had better pore sizes and distribution than the TMCS-silylated SA (Fig. 5b).

3.2 Effects of TMCS on chemical properties

Figure 6 shows a stacked plot of the FTIR spectra comparing the changes in the surface chemistries between the SA samples. Important characteristic peaks have been labeled accordingly. The basic surface chemistries of SA are based on siloxane groups (–Si–O–Si–) and silanol groups (–Si–OH). All samples showed three distinct silicone-oxygen characteristic peaks as observed near 470 cm^{-1}, 800 cm^{-1}, and 1100 cm^{-1}, respectively, corresponding to distinct modes of O–Si–O, Si–O, and Si–O–Si stretching vibrations [19, 20]. Changes in the FTIR spectra owing to TMCS surface modification can be noticed on the silylated SA samples, as shown by three new infrared peaks at around 850 cm^{-1}, 1260 cm^{-1}, and 2965 cm^{-1}. These peaks are attributed to the trimethylsilyl (Si–CH$_3$) groups of the Si–C, Si–CH$_3$, and C–H bonds, respectively. The peaks near 3450 cm^{-1} and 1640 cm^{-1} correspond to the vibrations of (–Si–OH) and (–OH) physisorbed water, respectively, which influence the hydrophilicity of the silica surface. The 0% TMCS sample showed a more intense (–Si–OH) absorption peak due to its hydrophilicity. Nevertheless, the (–Si–OH) peaks were still evident after 2%,

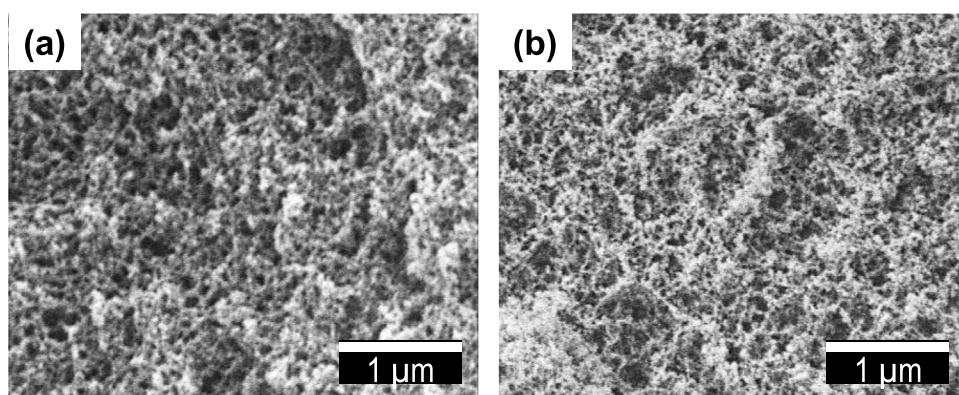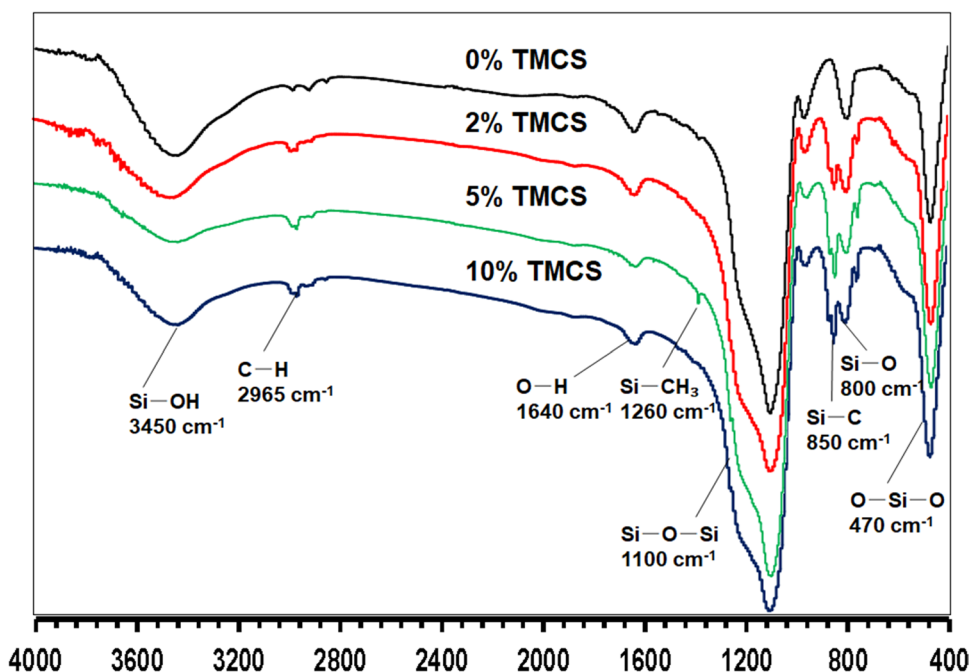**Fig. 5** SEM images of **a** original SA (0% %TMCS) and **b** 10% TMCS SA

Fig. 6 FTIR spectra of SA samples of different TMCS treatment

5%, and 10% TMCS modification, although their intensities were slightly decreased. This is unsurprising due to the fact that the TMCS did not entirely react with silanols, but instead chemisorbed selectively on free or terminal silanols, as previously discussed in other studies [21]. It is reported that surface hydrophobicity can be achieved by replacing more than half of the silanols on the surface of silica with non-polar groups from TMCS [22].

Meanwhile, a noticeable effect of TMCS was also seen on the pattern (i.e., intensity and resolution) of the siloxane absorption peak at 1100 cm^{-1}. A broader siloxane peak indicates a more branching and dense (–Si–O–Si–) network, whereas a greater intensity indicates a stronger Si–O bond arrangement [23]. The difference in the pattern of the (-Si-O-Si-) peaks in response to the TMCS% is caused by interaction between TMCS groups and free silanols during silylation. This resulted in the irreversible reconstruction of the siloxane bridge as well as changes in the SA's structural properties (i.e., pores and surface area) [22]. In this context, Fig. 7 illustrates the relationship between changes in siloxane absorption peaks to the physical structure of SA as a function of TMCS %. The change in siloxane absorption peak is indicated by its full-width half maximum (FWHM). Meanwhile, the structural parameter of the SA samples is represented by specific surface area per unit volume (SSAV). This is in accordance to Beer-Lambert Law [24], which relates the FTIR spectrum absorbance to the sample concentration and thickness. The SSAV is calculated by multiplying the specific surface area (m^2/g) by the density of the SA (g/cm^3), as expressed in m^2/cm^3 units. Our findings in Fig. 7 show that the FWHM is inversely related to the SSAV, implying that the broadening of the siloxane peak (higher FWHM) actually indicates a decrease in internal surface area per unit volume (i.e., pore volume). With 0% TMCS as

reference, the plot's value for the 5% TMCS exhibited the least change when compared to other samples, showing the least structural changes.

Other than the siloxane bond, we have also studied the bands linked with the Si–C bonds and the Si–OH groups of due to their connection to surface polarity. Previous research [16, 25, 26] demonstrated that the intensity ratios of the Si–C/Si–OH peaks could be used to determine the effectiveness of surface modification process (i.e., degree of silylation/hydrophobicity). In relation to this, Fig. 8 depicts the degree of silylation which is the intensity ratio between the Si–C peak at 850 cm^{-1} and the Si–OH peak near 3450 cm^{-1}. The ratio for the 0% TMCS was "0" since there is no Si–C peak evident in the sample's spectra. The 5% TMCS sample showed the highest Si–C/Si–OH ratio, indicating the most effective silylation, which is defined as the most substitution of the terminal hydroxyls
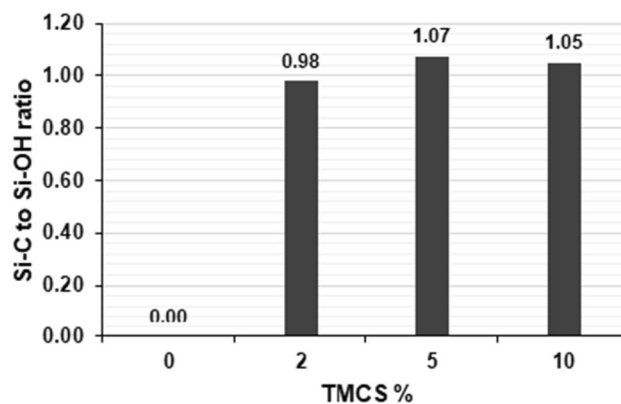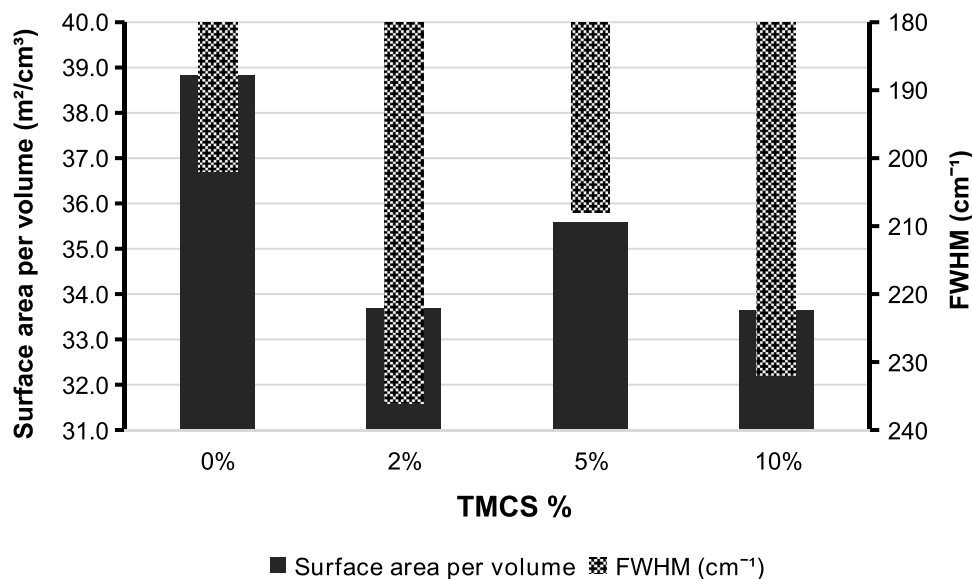

Fig. 8 Effective silylation based on the FTIR peak intensity ratio as a function of TMCS %

Fig. 7 Correlation between siloxane broadening and SA structure (SSAV) as a function of TMCS %

on the SA surface by the Si–CH$_3$ groups. However, as the TMCS concentration increased to 10%, the Si–C/Si–OH ratio decreased, implying that the degree of silylation had already exceeded its saturation point, beyond which no more silylation could occur [27, 28]. It was reported that only about 60% of the silanols (mainly isolated Si–OH) could have reacted with the silane, while the rest would have remained unbonded due to their inaccessibility to the reagent once the surrounding groups had reacted [29, 30].

3.3 Surface hydrophobicity, thermal conductivity, and thermal stability

Surface hydrophobicity is demonstrated by water droplet contact angles on surfaces coated with various SA samples as depicted in Fig. 9. Droplets of water are more clearly defined on a hydrophobic surface with contact angles greater than 90°. The contact angle of water droplets with the surface increases as their hydrophobicity increases. The water droplet on the original SA-coated surface has a contact angle of 20 ± 2.0°, demonstrating stronger interaction of water with the surface than the cohesive forces among water molecules, implying its hydrophilicity. In contrast, water droplets on surfaces coated with TMCS-modified SA have larger contact angles, indicating lower surface energy. The water contact angles for 2% TMCS, 5% TMCS, and 10% TMCS samples were 128 ± 2.0°, 140 ± 2.0°, and 136 ± 2.0°, respectively, confirming their surfaces as hydrophobic. This result is expected due to the fact

that the surface hydrophobicity is proportional to the degree of silylation, as was explained previously in Fig. 8.

Meanwhile, the average thermal conductivity of SA samples as determined by the hot-disk method is depicted in Fig. 10. Thermal conductivity is averaged from three independent measurements, the line plots show error bars for the standard deviation. The thermal conductivity of the original SA (0% TMCS), was measured to be 0.035 ± 0.002 W/mK. This value is close to that of traditional insulating materials such as mineral wool but SA has the advantage of high thermal resistance value (*R*-value) [31], due to its low density and large surface area. Subsequently, it was observed that the thermal conductivity of the TMCS-silylated SA had increased slightly as a result of structural shrinkage. Nonetheless, this is not surprising and is in accordance with previous findings, because the thermal insulation of aerogels is primarily determined by the morphology of their pores, while heat conduction through the skeletal network of silica nanoparticles contributes the most to total thermal conductivity. One example of a recent study [32], which evaluated the shrinking of the SA structure as a result of heat treatment found a similar increase in thermal conductivity with shrinkage and density. The dependence of thermal conductivity on shrinkage could also be observed in Fig. 10. It is clear that the thermal conductivity changes ($\Delta\lambda$), as determined based on the relative increase in thermal conductivity, were proportional to the rate of shrinkage as a function of TMCS concentration (%).
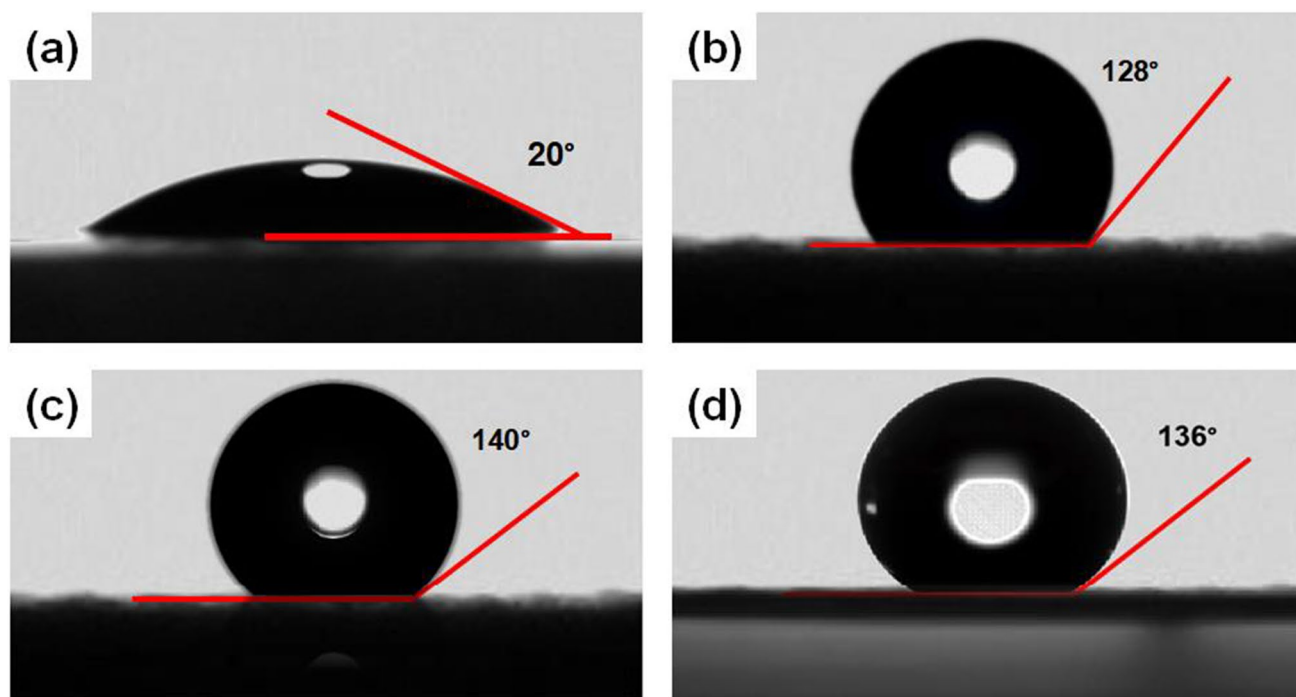

Fig. 9 Water contact angle measurement **a** original SA (0% TMCS), **b** 2% TMCS, **c** 5% TMCS, and **d** 10% TMCS
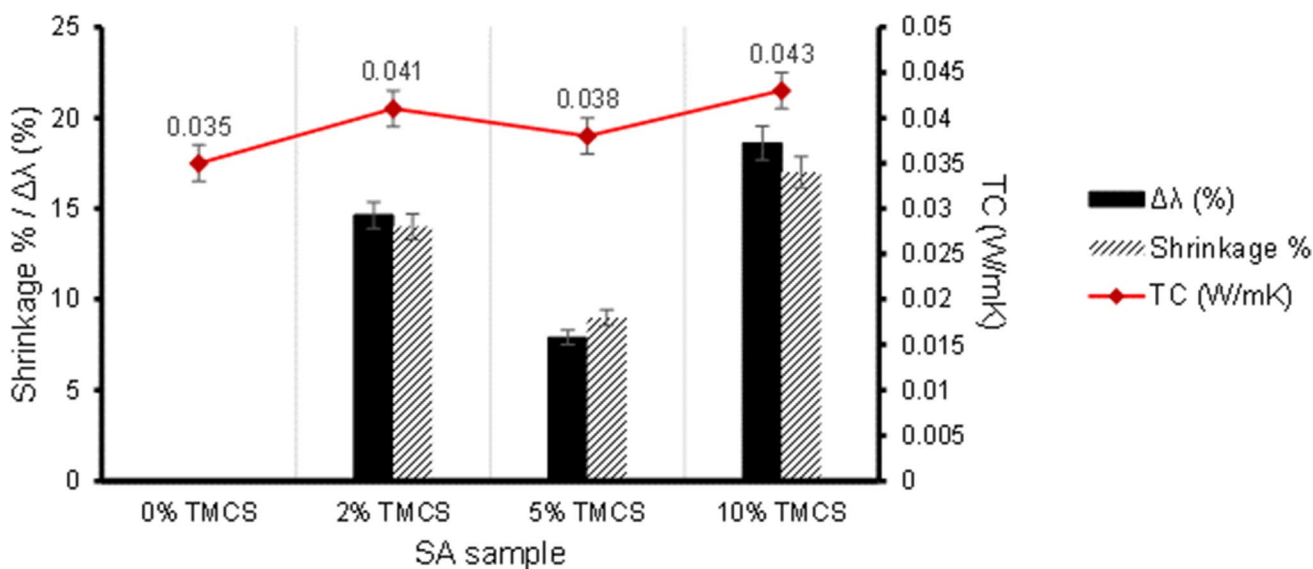
Fig. 10 Thermal conductivity (TC) of SA samples as a function of TMCS % (stacked line). The column chart depicts the correlation between the thermal conductivity changes (Δλ) and shrinkage

Lastly, thermal stability was measured for 5% TMCS sample as the most promising sample. Figure 11 compares the oxidative thermal stability of hydrophilic (0% TMCS) and hydrophobic SA (5% TMCS) up to 600 °C. The TG curve for the original SA (Fig. 11a) exhibits a slow weight loss (e.g., 3%) until around 400 °C, which has been attributed to the slow evaporation of trapped moisture and solvent from the pores. Following that, a 10% weight loss was observed up to 600 °C, resulting in a DTG peak at 420 °C. The broad DTG peak reflects the removal of non-hydrolyzed organic groups linked to the silica structure, such as the ethyl group

($-CH_2CH_3$), as well as the gradual breakdown of silanols from the silica surface, resulting in changes in pore morphology [33]. The hydrophobic SA, on the other hand, has greater thermal stability below 350 °C, as demonstrated in Fig. 11b. Initial weight loss for the 5% TMCS was insignificant up to 350 °C, as demonstrated by a low or non-existent slope in the TG/DTG curve, indicating that the SA contains no moisture. Following that, an extremely abrupt event occurred near 350 °C, resulting in a weight loss of approximately 4.5%, and the corresponding DTG peak is sharp due to the phase transition at constant temperature, that marks the loss
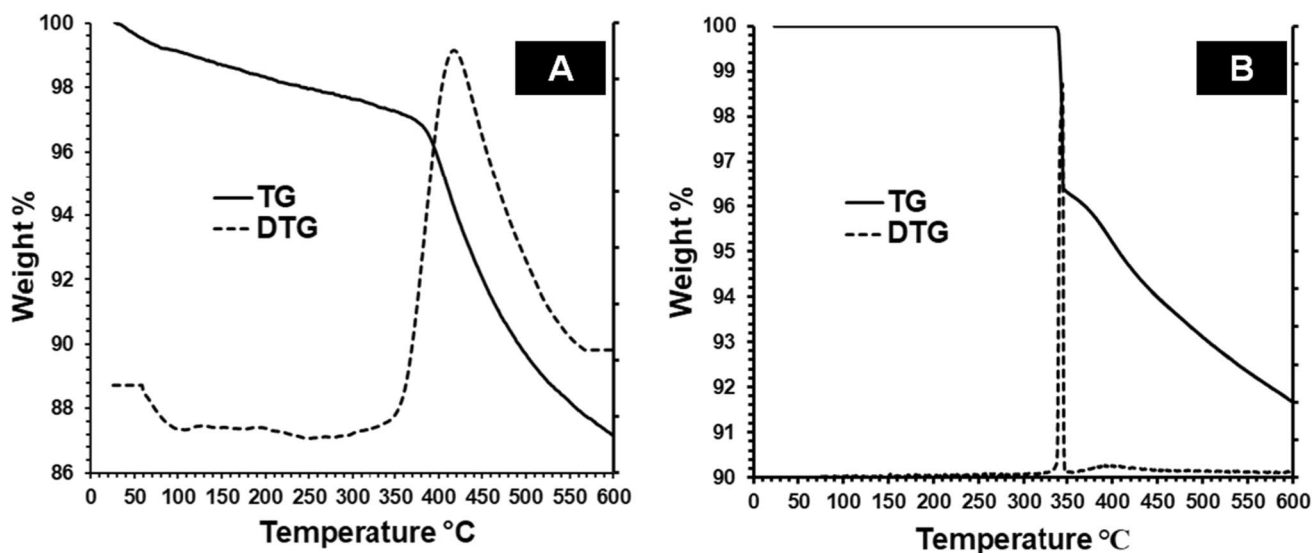

Fig. 11 TG and DTG curves of **a** original SA (hydrophilic) **b** 5% TMCS SA (hydrophobic)

of hydrophobicity. Similar to previous findings, this phase transition involves the oxidation of organic silyl groups (CH_3) on the silica surface, which results in the generation of carbon dioxide and water [34]. Above 350 °C, a gradual weight loss was observed until 600 °C, which was attributed to the removal of water by-products, followed by the elimination of residual hydroxyls from the SA surface, together with a reduction of the surface area [35]. In comparison, the total weight loss for hydrophilic SA from room temperature to 600 °C is nearly 13%, while hydrophobic SA is just under 8%.

4 Conclusion

An effective synthesis technique for hydrophobic SA particles employing RHA derived sodium silicate was proposed, eliminating the need for large volumes of solvent and silylating agent. First, SA particles with hydrophilic surfaces were synthesized using the ethanol SCFD technique. The SCFD was chosen because of its efficient process, which results in high-quality SA with good reproducibility. The SA particles as obtained from the SCFD process had a bulk density of 0.070 g/cm^3, a specific surface area of 715 m^2/g, and a thermal conductivity of 0.035 W/mK. The SA was then immersed in a silylating mixture containing small concentrations of TMCS, which are 2, 5, and 10% (by volume) in n-hexane. This silylation process is simpler and cheaper than the traditional APD method since it is a one-step process that requires only a small amount of TMCS to achieve hydrophobicity. The impact of TMCS concentration on the physicochemical properties of TMCS-silylated SA was investigated. Conversion of hydrophilic SA to hydrophobic was successful but at the trade-off of slight structural shrinkage and increased thermal conductivity. Our results showed that silylation was most effective at 5% TMCS, showing that raising the TMCS concentration does not always result in increased hydrophobicity. The 5% TMCS has the highest BET surface area (664 m^2/g), the lowest density (0.076 g/cm^3), the lowest thermal conductivity (0.038 W/mK), and the highest water contact angle (140°). The hydrophobic SA demonstrated better thermal stability than the hydrophilic (original SA) SA, and it can be maintained hydrophobic up to 350 °C.

Author contribution All authors contributed to the study conception and design. Material preparation, data collection, and analysis were performed by Zulhelmi Alif Abdul Halim and Muhamad Azizi Mat Yajid. The first draft of the manuscript was written by Nuha Awang and all authors commented on previous versions of the manuscript. All authors read and approved the final manuscript.

Data availability The datasets generated during and/or analyzed during the current study are available from the corresponding author on reasonable request.

Declarations

Competing interests The authors declare no competing interests.

References

1. Romasanta RR, Sander BO, Gaihre YK, Alberto Ma C, Gummert M, Quilty J, Nguyen VH, Castalone AG, Balingbing C, Sandro J, Correa T, Wassmann R (2017) How does burning of rice straw affect CH4 and N2O emissions? A comparative experiment of different on-field straw management practices. Agric Ecosyst Environ 239:143–153. https://doi.org/10.1016/j.agee.2016.12.042
2. Nazar M, Yasar A, Raza SA, Ahmad A, Rasheed R, Shahbaz M, Tabinda AB (2021) Techno-economic and environmental assessment of rice husk in comparison to coal and furnace oil as a boiler fuel. Bio Convers Bioref. https://doi.org/10.1007/s13399-020-01238-3
3. Gautam N, Athira Merlin Rose KV, Chaurasia A (2022) Study on chemical kinetics and characterization of nanosilica from rice husk and rice straw in the fixed-bed pyrolysis process. Bio Convers Bioref 12(5):1435–1448. https://doi.org/10.1007/s13399-020-00838-3
4. Nguyen PTT, Do NHN, Goh XY, Goh CJ, Le Ong RH, PK, Phan-Thien N and Duong HM, (2021) Recent progresses in eco-friendly fabrication and applications of sustainable aerogels from various waste materials. Waste Bio Valorization 13:1825–1847. https://doi.org/10.1007/s12649-021-01627-3
5. Abbas N, Khalid HR, Ban G, Kim HT, Lee HK (2019) Silica aerogel derived from rice husk: an aggregate replacer for lightweight and thermally insulating cement-based composites. Constr Build Mater 195:312–322. https://doi.org/10.1016/j.conbuildmat.2018.10.227
6. Adhikary SK, Ashish DK, Rudžionis Ž (2021) Aerogel based thermal insulating cementitious composites: a review. Energy and Buildings 245:111058. https://doi.org/10.1016/j.enbuild.2021.111058
7. Schmidt M, Schwertfeger F (1998) Applications for silica aerogel products. J Non-Cryst Solids 225:364–368. https://doi.org/10.1016/S0022-3093(98)00054-4
8. Perrut M (2000) Supercritical fluid applications: industrial developments and economic issues. Ind. Eng Chem Res 39(12):4351–4353. https://doi.org/10.1021/ie000211c
9. Błaszczyński T, Ślosarczyk A, Morawski M (2013) Synthesis of silica aerogel by supercritical drying method. Proc Eng 57:200–206. https://doi.org/10.1016/j.proeng.2013.04.028
10. Cheng Y, Li N, Wei C (2016) Effect of the TMCS/hydrogel volume ratio on physical properties of silica aerogels based on fly ash acid sludge. J Sol-Gel Sci Technol 78(2):279–284. https://doi.org/10.1007/s10971-015-3954-3
11 Wang L, Zhao S (2009) Synthesis and characteristics of mesoporous silica aerogels with one-step solvent exchange/surface modification. J Wuhan Univ Technol-Mater Sci Ed 24(4):613–618. https://doi.org/10.1007/s11595-009-4613-8

12. Feng Q, Chen K, Ma D, Lin H, Liu Z, Qin S, Luo Y (2018) Synthesis of high specific surface area silica aerogel from rice husk ash via ambient pressure drying. Colloids Surf, A 539:399–406. https://doi.org/10.1016/j.colsurfa.2017.12.025

13. Zhu L, Wang Y, Cui S, Yang F, Nie Z, Li Q, Wei Q (2018) Preparation of silica aerogels by ambient pressure drying without causing equipment corrosion. Molecules 23(8):1935. https://doi.org/10.3390/molecules23081935

14. Yi Z, Tang Q, Jiang T, Cheng Y (2019) Adsorption performance of hydrophobic/hydrophilic silica aerogel for low concentration organic pollutant in aqueous solution. Nanotechnol Rev 8(1):266–274. https://doi.org/10.1515/ntrev-2019-0025

15. He S, Huang D, Bi H, Li Z, Yang H, Cheng X (2015) Synthesis and characterization of silica aerogels dried under ambient pressure bed on water glass. J Non-Cryst Solids 410:58–64. https://doi.org/10.1016/j.jnoncrysol.2014.12.011

16. Bangi UKH, Rao AV, Rao AP (2008) A new route for preparation of sodium-silicate-based hydrophobic silica aerogels via ambient-pressure drying. Sci Technol Adv Mater 9(3):035006. https://doi.org/10.1088/1468-6996/9/3/035006

17. Nah HY, Parale VG, Lee KY, Choi H, Kim T, Lim CH, Seo JY, Ku YS, Park JW, Park HH (2018) Silylation of sodium silicate-based silica aerogel using trimethylethoxysilane as alternative surface modification agent. J Sol-Gel Sci Technol 87:319–330. https://doi.org/10.1007/s10971-018-4729-4

18. El-Sakhawy M, Adel AM, Diab MA, Al-Shemy M (2020) Facile methods for the preparation of micro- and mesoporous amorphous silica from rice husk. Biom Convers Bioref 12:4709–4718. https://doi.org/10.1007/s13399-020-01112-2

19. Bergna HE (1994) Colloid chemistry of silica. Colloid Chem Silica 234:1–47. https://doi.org/10.1021/ba-1994-0234.ch001

20. Nayak PP, Datta AK (2022) An entropy-based TOPSIS approach for selecting best suitable rice husk for potential energy applications: pyrolysis kinetics and characterization of rice husk and rice husk ash. Bio Convers Bioref. https://doi.org/10.1007/s13399-022-02824-3

21. Eslava S, Delahaye S, Baklanov MR, Iacopi F, Kirschhock CEA, Maex K, Martens JA (2008) Reaction of trimethylchlorosilane in spin-on silicalite-1 zeolite film. Langmuir 24(9):4894–4900. https://doi.org/10.1021/la800086y

22. Cyran JD, Donovan MA, Vollmer D, Siro Brigiano F, Pezzotti S, Galimberti DR, Gaigeot M-P, Bonn M, Backus EHG (2019) Molecular hydrophobicity at a macroscopically hydrophilic surface. Proc Natl Acad Sci 116(5):1520–1525. https://doi.org/10.1073/pnas.1819000116

23. Darmawan A, Rasyid SA, Astuti Y (2021) Modification of the glass surface with hydrophobic silica thin layers using tetraethylorthosilicate (TEOS) and trimethylchlorosilane (TMCS) precursors. Surf Interface Anal 53(3):305–313. https://doi.org/10.1002/sia.6917

24. Liu H, Liu J, Tian Y, Jiao J, Wu X (2022) Thermal insulation performance of silica aerogel composites doped with hollow opacifiers: theoretical approach. Gels 8(5):295. https://doi.org/10.3390/gels8050295

25. Rao V, Kalesh R (2003) Comparative studies of the physical and hydrophobic properties of TEOS based silica aerogels using different co-precursors. Sci Technol Adv Mater 4(6):509–515. https://doi.org/10.1016/j.stam.2003.12.010

26. Khedkar MV, Jadhav SA, Somvanshi SB, Kharat PB, Jadhav KM (2020) Physicochemical properties of ambient pressure dried surface modified silica aerogels: effect of pH variation. SN Applied Sciences 2(4):696. https://doi.org/10.1007/s42452-020-2463-3

27. Jung S-B, Park H-H (2002) Control of surface residual OH polar bonds in SiO2 aerogel film by silylation. Thin Solid Films 420–421:503–507. https://doi.org/10.1016/S0040-6090(02)00835-0

28. Prakash SS, Brinker CJ, Hurd AJ, Rao SM (1995) Silica aerogel films prepared at ambient pressure by using surface derivatization to induce reversible drying shrinkage. Nature 374(6521):439–443. https://doi.org/10.1038/374439a0

29. Cox GB (1993) The influence of silica structure on reversed-phase retention. J Chromatogr A 656(1):353–367. https://doi.org/10.1016/0021-9673(93)80809-M

30. Bair MD, Dorsey JG (2012) Effect of trimethylsilane pre-capping on monomeric C18 stationary phases made from high-purity type-B silica substrates: efficiency, retention, and stability. J Chromatogr A 1220:35–43. https://doi.org/10.1016/j.chroma.2011.11.041

31. Schiavoni S, D'Alessandro F, Bianchi F, Asdrubali F (2016) Insulation materials for the building sector: a review and comparative analysis. Renew Sustain Energy Rev 62:988–1011. https://doi.org/10.1016/j.rser.2016.05.045

32. Lun Z, Gong L, Zhang Z, Deng Y, Zhou Y, Pan Y, Cheng X (2022) Improvement of the thermal insulation performance of silica aerogel by proper heat treatment: microporous structures changes and pyrolysis mechanism. Gels 8(3):141. https://doi.org/10.3390/gels8030141

33. Li Z, Cheng X, Shi L, He S, Gong L, Li C, Zhang H (2016) Flammability and oxidation kinetics of hydrophobic silica aerogels. J Hazard Mater 320:350–358. https://doi.org/10.1016/j.jhazmat.2016.07.054

34. Halim ZAA, Yajid MAM, Hamdan H (2020) Effects of solvent exchange period and heat treatment on physical and chemical properties of rice husk derived silica aerogels. Silicon 13:251–257. https://doi.org/10.1007/s12633-020-00421-5

35. Fermino TZ, Awano CM, Moreno LX, Vollet DR, de Vicente FS (2018) Structure and thermal stability in hydrophobic Pluronic F127-modified silica aerogels. Microporous-Mesoporous Mater 267:242–248. https://doi.org/10.1016/j.micromeso.2018.03.039